Journal of Applied Electrochemistry **34**: 1191–1197, 2004.

Impedance of a rotating disc electrode with a reversible reaction

M. BOILLOT[1], S. DIDIERJEAN[2] and F. LAPICQUE[1]*
[1]*Laboratoire des Sciences du Génie Chimique, CNRS-ENSIC, F-54001 Nancy, France*
[2]*Laboratoire d'Energétique, de Mécanique et Thermique Appliquées, CNRS-INPL-UHP, 54500 Vandoeuvre les Nancy, France*
*(*author for correspondence, e-mail: francois.lapicque@ensic.inpl-nancy.fr)*

Received 5 December 2003; accepted in revised form 19 April 2004

Key words: charge transfer resistance, hexacyanoferrate, impedance measurements, modelling

Abstract

This paper presents a model of electrode impedance for the case of a fast reversible reaction. The various contributions of the impedance were analysed with particular emphasis on the charge transfer resistance: this resistance was shown to be also dependent on mass transfer phenomena. For the case of significant mass transfer control, the diameter of the high-frequency loop increases with the absolute value of the overpotential. The various physicochemical parameters involved in the expression for impedance were determined through previous measurements. The impedance model was validated by experimental measurements carried out with the hexacyanoferrate (II)–(III) couple on a Pt RDE.

List of symbols

D diffusion coefficient ($m^2\,s^{-1}$)
E potential (V)
F faradaic constant = 96 487 $C\,mol^{-1}$
f $F/(RT)$(V^{-1})
i current density ($A\,m^{-2}$)
i_0 exchange current density ($A\,m^{-2}$)
I current (A)
j imaginary number ($j^2 = -1$)
m average of the relative deviation
n constant phase element (CPE) parameter
N number of frequencies in spectra
Q specific generalised capacitance ($\Omega^{-1}\,s^n\,cm^{-2}$)
r specific resistance ($\Omega\,m^2$)
R gas constant (8.314 $J\,K^{-1}\,mol^{-1}$)
R resistance (Ω)
R_e cell resistance (Ω)
s Laplace variable (s^{-1})
t time (s)
T temperature (K)
x distance from the electrode surface (m)
[X] concentration of species X ($mol\,m^{-3}$)
z specific impedance ($\Omega\,m^{-2}$)
Z impedance (Ω)
Z' real part of the impedance (Ω)
Z'' imaginary part of the impedance (Ω)

Greek symbols

α charge transfer coefficient
δ thickness of the diffusion layer (m)
η electrode overpotential (V)
ρ density of the solution ($kg\,m^{-3}$)
ν kinematic viscosity of the solution ($m^2\,s^{-1}$)
ω signal pulsation ($rad\,s^{-1}$)
Ω angular velocity of the electrode ($rad\,s^{-1}$)

Subscripts

c concentration
f faradaic
L limiting
Ox oxidant
Red reductant
ct charge transfer
∞ in the bulk
0 at the electrode surface

Exponent

$\hat{}$ model

1. Introduction

The kinetics of electrochemical processes occurring at an electrode surface are often described by the Butler–Volmer equation, or by derived laws accounting for diffusion of species or successive electron transfer. The deduced expression for the current density is then used to establish the expression for electrode impedance. This expression takes into account the time variations of

several variables, namely the electrode potential, the surface charge and the species concentrations. It is often considered that the high-frequency part of impedance spectra allows estimation of the ohmic resistance of the cell, and the charge transfer resistance. Pulsation of concentration profiles near the electrode surface is also visible at low frequencies only, and corresponds to the Warburg impedance for finite or infinite diffusion.

The potential and concentration dependence of the charge transfer resistance was treated in the pioneering, extensive work of Sluyters-Rehbach [1], and the approach is also detailed in [2]. However, in most published work, the diffusion of species to and from the electrode surface is neglected in the high frequency part of the spectrum: this assumption is only valid for current densities far below the limiting current density. In contrast, most investigations of Warburg impedances do not take into account the charge transfer overpotential, and the expressions given are often established at the equilibrium potential [3–6].

Although the problem has been treated previously, the present work was aimed at establishing the general expression for the impedance of a simple electrochemical system. The various contributions of the impedance were analysed, with particular attention to the resistance related to the high frequency loop. Investigations were made for the reversible potassium hexacyanoferrate (II) and (III) couple at the surface of a platinum RDE. The concentration profiles were assumed to be due to diffusion only, and the charge transfer rate was expressed by the Butler–Volmer relationship. The various physicochemical parameters involved in the model were found by experiment. The predicted spectra were validated by impedance measurements.

2. Current–potential relationship

2.1. *Experimental details*

The reaction considered was the reversible reduction of potassium hexacyanoferrate (III) in alkaline solution on platinum. The electrolyte solution was $10\,\mathrm{mol\,m^{-3}}$ $K_3Fe(CN)_6$, $100\,\mathrm{mol\,m^{-3}}$ $K_4Fe(CN)_6$, $500\,\mathrm{mol\,m^{-3}}$ NaOH medium. All reagents were of analytical grade (Normapur, Prolabo, France). All measurements were carried out at 24 °C within 0.5 °C. The solution viscosity was interpolated from published data at $0.92\times10^{-6}\,\mathrm{m^2\,s^{-1}}$. Diffusion coefficients of the two ions were estimated from tabulated data [7, 8], and using the Nernst–Einstein relation ($D\mu/T$ = constant) for temperature correction. Values of 8.35 and $6.87\times10^{-10}\,\mathrm{m^2\,s^{-1}}$ were obtained for Fe(II) and Fe(III), respectively.

The electrode was a platinum disc with a radius of 1.0 mm, embedded in a PTFE shaft of 11 mm diameter. The platinum surface was carefully polished using diamond pastes with decreasing mesh sizes. The surface was cleaned with conductivity water, then ethyl alcohol, and water again. The surface was activated by oxygen evolution at 1 mA for 1 min, then hydrogen evolution at 2 mA for 10 min. Electrochemical measurements were carried out in a standard three-electrode cell. A platinum basket acted as counter electrode and the reference electrode was a Pt wire (6.0332.000 Metrohm). An Autolab PGSTAT 20 controlled by GPES 4.4 software was used for steady-state measurements. Voltammograms were recorded in the range from 0 to −150 mV at $2.5\,\mathrm{mV\,s^{-1}}$. Numerous replicates were made to control the repeatability of the measurements. After each scan, the electrode surface was cleaned using a fine paper cloth wetted with conductivity water. In addition, tests carried out at $1\,\mathrm{mV\,s^{-1}}$ did not result in significant changes in i/E variations, and the curves recorded at the usual rate were assumed to be representative of steady-state conditions.

The rotation rate was varied as follows: the reference rotation rate was 300 rpm and three other rates were also used: 670, 1220 and 1850 rpm, allowing the limiting current to be 1.5, 2.0 and 2.5 as large as the reference limiting current, after the Levich relationship. Experimental curves are shown in Figure 1.

2.2. *Steady-state i/E law*

The electrochemical reaction is written as

$$\mathrm{Ox} + \mathrm{e^-} \longleftrightarrow \mathrm{Red} \tag{1}$$

where Ox is Fe(III) species, and Red is for Fe(II). The current–voltage relationship was established considering the rates of both the reduction (forward reaction), and the oxidation (reverse process), and introducing the exchange current density, i_0, defined on the basis of the bulk concentrations. Taking into account the existence of the concentration profiles near the electrode surface, the faradaic current density is written as

$$i_f(t) = i_0\left[\frac{[\mathrm{Red}]_{0,t}}{[\mathrm{Red}]_\infty}\exp\left(\frac{\alpha F}{RT}\eta(t)\right) - \frac{[\mathrm{Ox}]_{0,t}}{[\mathrm{Ox}]_\infty}\exp\left(-\frac{(1-\alpha)F}{RT}\eta(t)\right)\right] \tag{2}$$

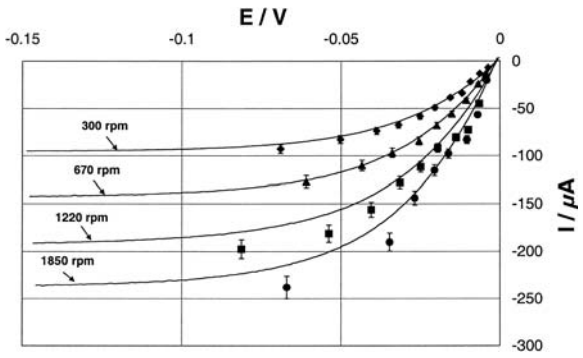

Fig. 1. Voltammetric curves of the reduction of hexacyanoferrate (III) at $5\,\mathrm{mol\,m^{-3}}$ on a 1 mm Pt RDE. Scanning rate $2.5\,\mathrm{mV\,s^{-1}}$. Rotation rates 300, 670, 1220 and 1850 rpm. Both experimental and fitted (i/E) are in solid lines. Symbols are for the current recorded during impedance measurements with 5% error bars.

where α is the charge transfer coefficient and η the overpotential. Subscripts 0 and ∞ are for the electrode surface and the bulk conditions, respectively. It can be observed that Relation 2 is valid for both steady state and non-steady condition.

At steady state, according to the Nernst film model, the concentration profiles are assumed to be linear. The concentration ratios appearing in Relation 2 can be expressed against the faradaic current density, with the limiting current densities of the two species, $i_{L,Red}$ and $i_{L,Ox}$:

$$\frac{[\mathrm{Red}]_0}{[\mathrm{Red}]_\infty} = 1 - \frac{i_f}{i_{L,\mathrm{Red}}} \tag{3a}$$

$$\frac{[\mathrm{Ox}]_0}{[\mathrm{Ox}]_\infty} = 1 + \frac{i_f}{i_{L,\mathrm{Ox}}} \tag{3b}$$

For the present case of a RDE, the limiting current densities were given by the Levich relationship written for large Sc numbers:

$$i_{L,\mathrm{Red}} = 0.621\, F D_{\mathrm{Red}}^{2/3} \nu^{-1/6} \Omega^{1/2} [\mathrm{Red}]_\infty \tag{4a}$$

$$i_{L,\mathrm{Ox}} = 0.621\, F D_{\mathrm{Ox}}^{2/3} \nu^{-1/6} \Omega^{1/2} [\mathrm{Ox}]_\infty \tag{4b}$$

where D_{Red} and D_{Ox} are the diffusion coefficients of the two species considered and Ω is the angular velocity in rad s^{-1}.

The faradaic current density at steady state is then expressed in the form of a generalized Butler–Volmer law. Moreover, the charge transfer coefficient is close to 0.5, as reported in various investigations, [eg., 9, 10]. Fixing α at 0.5 simplifies the expression. Thus,

$$i_f = \frac{2 i_0 \sinh(0.5 f \eta)}{1 + i_0 \left[\frac{\exp(0.5 f \eta)}{i_{L,\mathrm{Red}}} + \frac{\exp(-0.5 f \eta)}{i_{L,\mathrm{Ox}}} \right]} \tag{5}$$

2.3. *Fitting of voltammetric curves*

The experimental curves were corrected for ohmic drop and fitted to Equation 5 taking into account the equilibrium potential. For this purpose, the cell resistance, R_e, was measured by impedance spectroscopy at 21.2 Ω within 1 Ω. The faradaic current density was calculated from the current recorded, assuming that the active area was equal to the geometric area. The exchange current density was obtained by minimization of the sum of the squared deviations between theoretical and experimental current densities, and the operation was conducted for the simultaneous fitting of the four i/E curves, i.e. with the four rotation rates considered:

$$i_0 = 826\ \mathrm{A\,m^{-2}} \tag{6}$$

Taking into account the bulk concentration of Fe(III) and neglecting the equilibrium potential involved in the expression for the exchange current density, this value corresponds to rate constants of the order of 0.05–0.1 cm s^{-1}, in agreement with the broad range 0.02–0.5 cm s^{-1} published [10]. The experimental data were perfectly fitted by Relation 5, with hardly visible difference between the two series of data, confirming that α can be taken at 0.5.

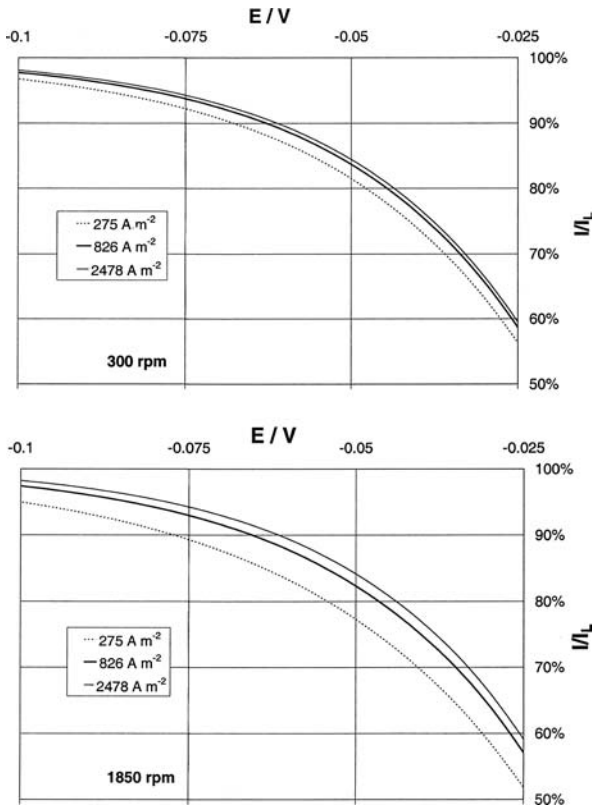

Fig. 2. Effect of the value for the exchange current density on the model predictions (Relation 5). Rotation rate 300 rpm (top) and 1850 rpm (bottom).

The determination of i_0 is nevertheless of moderate accuracy. Estimation of a confidence interval for i_0 could not been carried out because Relation 5 is far from linear. The effect of the exchange current density on (i/E) variations was assessed by considering three levels for i_0: $i_0 = 826\ \mathrm{A\,m^{-2}}$, $i_{0,\max} = 3\, i_0$, and $i_{0,\min} = i_0/3$. Results are shown in Figure 2 for 300 and 1850 rpm. Increasing i_0 by a factor of 3 is of little effect on the current profiles; in contrast, simulations with $i_{0,\min}$ (275 A m^{-2}) resulted in noticeable differences, in particular for the highest rotation rates. The influence of the rotation rate was expected since the reaction is more controlled by charge transfer rate at high rotation speeds.

3. Impedance spectroscopy

3.1. *Experimental details*

Impedance spectra were recorded after voltammetric measurements, with the aid of FRA 2.9 software for electrical control in sine mode and data acquisition. The

electrode impedance was measured in potensiostatic mode, with a specific procedure developed for fast electrode kinetics, as follows. The steady potential to be applied was determined as corresponding to a specified current, using a trial-and-error procedure. The ratio of the current to the limiting current for species Ox, $(I/I_{L,Ox})$ was varied from 10% to 90%. The potential fluctuation fixed at 5% of the steady potential, was in the range 0.5–3 mV. The frequency was varied from 10 kHz to 10 mHz at 300 rpm, and to 100 mHz at higher rotation rates. Ten frequencies per decade were used. The electrode surface was cleaned after each spectrum, as explained in Section 2.1.

The steady value of the current was averaged over the acquisition time and the (I/E) couples obtained for impedance measurement were compared to the voltammetric curves. Figure 1 shows acceptable agreement between the two sources of data within 5% for most cases, as indicated by the error bars. Nevertheless, appreciable discrepancy was observed for the two highest rotation rates, at high fractions of the limiting current. Analysis of the raw data obtained for the above conditions revealed variations of the steady potential up to 10% during the acquisition. This may be due to partial blockage of the platinum surface by adsorption of hexacyanoferrate ions or their decomposition products, or to non-uniform distributions of current and potential at the electrode [11].

The spectra recorded exhibited expected Nyquist profiles (Figure 3), with a fraction of a high-frequency loop, followed by a 45° straight line observed from 500 to 25 Hz, bending into half-a circle at lower frequencies, corresponding to finite diffusion near the electrode surface.

3.2. *Expression of the electrode impedance*

For the present case, the faradaic current density depends on three variables: E and the interfacial concentrations of Ox and Red. First order expansion of the faradaic current density with respect to the three variables yielded the expression for its deviation around the steady operating point:

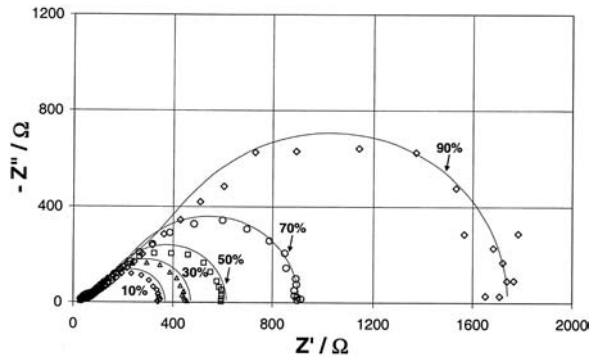

Fig. 3. Experimental (symbols) and theoretical impedance spectra (solid lines) recorded from 10 kHz to 10 mHz for various $(I/I_{L,Ox})$ ratios. Rotation rate 300 rpm.

$$\Delta i_f = \left(\frac{\partial i_f}{\partial E}\right)_{[Red]_0,[Ox]_0} \Delta E + \left(\frac{\partial i_f}{\partial [Red]_{0,t}}\right)_{E,[Ox]_0} \Delta [Red]_{0,t} + \left(\frac{\partial i_f}{\partial [Ox]_{0,t}}\right)_{E,[Red]_0} \Delta [Ox]_{0,t} \quad (7)$$

Relation 7 was written in Laplace domain, with barred variables. The partial derivatives are related to steady state. For clarity, subscripts in the partial derivatives are omitted below. The specific faradaic impedance was defined as the ratio of the potential variation to that of the current density:

$$z_f = \frac{\Delta \overline{E}}{\Delta \bar{i}_f} = \left(\frac{\partial E}{\partial i_f}\right) - \left(\frac{\partial i_f}{\partial [Red]_0}\right)\left(\frac{\partial E}{\partial i_f}\right)\frac{\Delta [\overline{R}ed]_{0,s}}{\Delta \bar{i}_f} - \left(\frac{\partial i_f}{\partial [Ox]_0}\right)\left(\frac{\partial E}{\partial i_f}\right)\frac{\Delta [\overline{O}x]_{0,s}}{\Delta \bar{i}_f} \quad (8)$$

The specific charge transfer resistance, r_{ct}, is the first contribution in the faradaic impedance:

$$r_{ct} = \left(\frac{\partial E}{\partial i_f}\right) = \left(\frac{\partial \eta}{\partial i_f}\right) \quad (9)$$

This specific resistance was derived by differentiating Relation 2 with respect to eta:

$$r_{ct} = \frac{1}{\alpha f i_0} \times \frac{1}{\left[\frac{[Red]_0}{[Red]_\infty}\exp(\alpha f \eta) + \frac{[Ox]_0}{[Ox]_\infty}\exp(-(1-\alpha) f \eta)\right]} \quad (10)$$

where the concentration ratios are given by Equations 3(a) and 3(b). Relation 10 clearly shows that the 'charge transfer resistance' is also related to mass transfer phenomena, and 'high frequency resistance' might be preferred for more rigorous expression.

The concentration resistances are the two last contributions in the faradaic impedance and are the products of three terms. Calculation of the derivatives of the current density with respect to the interfacial concentrations is straightforward. The ratios of the concentration deviations to the current density deviations were also calculated from differential mass balances in the liquid [3, 4]. The rigorous treatment of convective flow in the vicinity of the rotating disc electrode in addition to diffusion, has been carried out, and analytic expressions for $(\Delta \overline{C}_0/\Delta \bar{i}_f)$ have been obtained [12–14]. However, implementation of the complex expression of $(\Delta \overline{C}_0/\Delta \bar{i}_f)$ in the overall impedance expression was beyond the aim of this work, and the convection term was neglected here. Therefore, for the case of species Red, the mass balance was reduced to

$$\frac{\partial [Red]_{x,t}}{\partial t} = D_{Red}\frac{\partial^2 [Red]_{x,t}}{\partial x^2} \quad (11)$$

subject to the following boundary conditions:

$$\begin{aligned} [\mathrm{Red}]_{x,t=0} &= [\mathrm{Red}]_{\infty} \\ [\mathrm{Red}]_{\delta,t} &= [\mathrm{Red}]_{\infty} \\ D_{\mathrm{red}}\left(\frac{\partial[\mathrm{Red}]_{x,t}}{\partial x}\right)_{x=0} &= \frac{i_{\mathrm{f}}}{F} \end{aligned} \tag{12}$$

Equations 11 and 12 were written in the Laplace domain, and integration of Equation 11 was carried out. Algebraic rearrangement yielded the expressions for the concentration impedance, and the specific faradaic impedance was expressed as follows:

$$z_{\mathrm{f}} = r_{\mathrm{ct}}\left(1 + \frac{i_0}{[\mathrm{Red}]_{\infty}}\exp(\alpha f\eta)\frac{\tanh\left(\frac{s^{1/2}\delta_{\mathrm{Red}}}{D_{\mathrm{Red}}}\right)}{FD_{\mathrm{Red}}^{1/2}s^{1/2}} + \frac{i_0}{[\mathrm{Ox}]_{\infty}}\exp(-(1-\alpha)f\eta)\frac{\tanh\left(\frac{s^{1/2}\delta_{\mathrm{Ox}}}{D_{\mathrm{Ox}}}\right)}{FD_{\mathrm{Ox}}^{1/2}s^{1/2}}\right) \tag{13}$$

where δ_{Red} and δ_{Ox} are the thickness of the diffusion layer for the two species, given by the Levich relationship. For impedance spectroscopy, s is replaced by $\mathrm{j}\omega$, where $\mathrm{j}^2 = -1$, and ω is the pulsation of the sine signal. At high frequencies, the two right-hand terms in the expression for z_{f} are insignificant, and z_{f} reduces to r_{ct}. Conversely, these contributions become predominant at low frequencies.

The total current through an electrode surface is the sum of the faradaic and capacitive contributions. The Randles circuit describing the electrode surface was the classical parallel combination of faradaic and capacitive impedances, in series with the ohmic resistance of the cell. Capacitive phenomena were described in the model by a CPE, with parameters Q and n:

$$z_{\mathrm{CPE}} = \frac{1}{(\mathrm{j}\omega)^n Q} \tag{14}$$

and the overall electrode impedance $\hat{z}$ is

$$\hat{z} = r_{\mathrm{e}} + \frac{z_{\mathrm{CPE}}z_{\mathrm{f}}}{z_{\mathrm{CPE}} + z_{\mathrm{f}}} \tag{15}$$

3.3. *Fitting of experimental data*

The parameters involved in the expression for z_{f} were determined by voltammetric measurements. The global impedance depends on the generalised capacitance Q and parameter n. The two of them were determined by fitting of the experimental impedance, Z, to the model predictions: theoretical impedance $\hat{Z}$ was deduced from $\hat{z}$ taking into account the geometrical area of the disc electrode. For the same couple (redox system–electrode material) n varies from 0.8 to 1 according to [15] and the generalized capacitance was reported to be near $20\,\mu\Omega^{-1}\,\mathrm{s}^n\mathrm{cm}^{-2}$ [11]. Fitting was conducted by minimisation of the relative deviations of the real and imaginary components, Z' and Z'', respectively. At fixed steady current and rotation rate, the two relative deviations were averaged over the number of frequencies, that is, $N = 60$ at 300 rpm, and $N = 50$. Otherwise,

$$\begin{aligned} m' &= \frac{1}{N}\sum_i \frac{|Z_i' - \hat{Z}_i'|}{\hat{Z}_i'} \\ m'' &= \frac{1}{N}\sum_i \frac{|Z_i'' - \hat{Z}_i''|}{\hat{Z}_i''} \end{aligned} \tag{16}$$

Calculations were made for all conditions investigated: m' and m'' were averaged over the currents and the rotation rates considered. For n higher than 0.85 the variations of the averages of m' and m'' with Q exhibited well-defined minima. Minimum values of the averaged values of m' and m'' were obtained with $n = 1$, and this value was thereafter selected. The average deviation of the real components was the lowest for $Q = 30\,\mu\mathrm{F\,cm}^{-2}$, whereas $50\,\mu\mathrm{F\,cm}^{-2}$ allowed the best fitting of the imaginary parts. The average value at $40\,\mu\mathrm{F\,cm}^{-2}$ was selected for the fitting, with $m' = m'' = 0.10$, and yielded satisfactory representation of the impedance loop (Figure 3). The observable deviation observed for $(i/i_{\mathrm{L,Ox}}) = 10$, 30 and 50% may be caused by the approximate expression for $(\Delta\overline{C}_0/\Delta\bar{i}_{\mathrm{f}})$. In addition, slight deviations in the frequency distribution were observed, as exemplified in Figure 4. This deviation may be due to the average value for Q used, which may slightly differ from the real capacitance in the considered experiment.

3.4. *Discussion*

3.4.1. *Quality of the fitting at high frequency*

Prediction of the high-frequency part of the spectrum was in some cases inaccurate. One significant error in the model originates from the uncertainty in the estimated exchange current density, as discussed above. It can be supposed that the actual exchange current density may change from one run to another, in spite of the careful electrode preparation. The electrode impedance was calculated for the three values of i_0 considered in Section 2.3, and the high frequency impedances obtained are

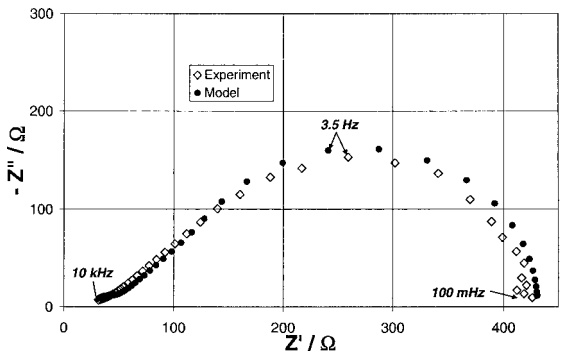

Fig. 4. Comparison of experimental and predicted impedance spectra. Rotation rate = 1850 rpm and $(I/I_{\mathrm{L,Ox}}) = 80\%$.

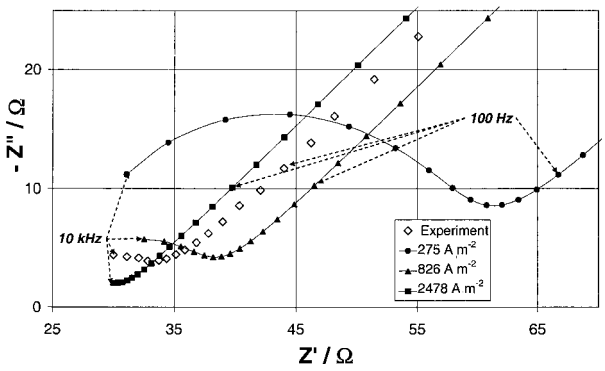

Fig. 5. High frequency part of impedance spectra: comparison of the experimental data to the predicted spectra with various values for i_0. Rotation rate 300 rpm and $(I/I_{L,Ox}) = 10\%$.

shown in Figure 5 for $i_f/i_{L,Ox} = 10\%$ and 300 rpm. Contrary to what was observed in voltammetry, i_0 exerts a strong effect on the first part of the spectrum: for $i_{0,max}$, the high-frequency loop is hardly visible below 10 kHz, whereas it is perfectly defined for the minimum value. The experimental spectrum could not be perfectly fitted by using $i_0 = 826\,A\,m^{-2}$ as given by voltammetry, and for the example considered, it appears that the actual exchange current density was somewhat larger than the selected value.

3.4.2. *High-frequency loop*

It is often considered that the high-frequency loop gives information on the charge transfer kinetics, whereas diffusion control is indicated by the low-frequency diagram. This statement is probably true for low values of i_0 in comparison to current densities $i_{L,Ox}$ and $i_{L,Red}$: such situation is frequently encountered in metal deposition or electrorganic synthesis. For such cases, the expression of the specific charge transfer resistance reduces to

$$r_{ct} = \frac{1}{\alpha i_0 f[\exp(\alpha f\eta) + \exp(-(1-\alpha)f\eta)]} \qquad (17)$$

For irreversible, slow reactions, the specific resistance r_{ct} is a decreasing function of the absolute overpotential $|\eta|$, and a log plot is often used for estimation of i_0 and α. In the present case, i_0 is larger than the two limiting current densities and, as shown in Figure 6, r_{ct} increases with the absolute overpotential, as indicated by Relation 10. In the case where i_0 and $i_{L,Ox}$ are of comparable order of magnitude, r_{ct} varies little with $|\eta|$. As the reaction becomes diffusion-controlled, r_{ct} increases with the overpotential, approaching the asymptotic function $\exp(-(1-\alpha)f|\eta|)$ at sufficient polarization.

3.4.3. *Low-frequency loop*

The overall impedance Z_f at nil frequency (i.e., at steady state) was deduced from the intercept of the impedance spectra with the real axis. The experimental data are fairly well predicted by the model (Figure 3). However, simulations conducted with the extreme estimates for i_0 yielded very similar impedance values: for these simulations the reduction is mainly diffusion-controlled, and the concentration impedance prevails over the charge transfer resistance for $|\eta|$ over a few millivolts. Steady-state Z_f increases with $|\eta|$, and at sufficient polarisation, the overall concentration impedance, Z_c, defined as $(Z_f - R_{ct} - R_e)$ approaches its asymptotic expression, as shown by the linear–log plot given in Figure 7: for $i_0 \gg i_{L,Ox}$, the plot tends to be linear with a slope of $2(1-\alpha)f$. Experimental data are fairly well represented by the model for Z_c, in spite of noticeable deviations at low overpotentials. Further simulations were made with lower i_0 values. The profile of the concentration impedance at steady state becomes more sensitive to the exchange current density for i_0 below $100\,A\,m^{-2}$ (Figure 7). In case that $i_0 \ll i_{L,Ox}$, Z_c at nil frequency increases with $|\eta|$ in a narrow overpotential range and attains a plateau as soon as the reaction becomes irreversible.

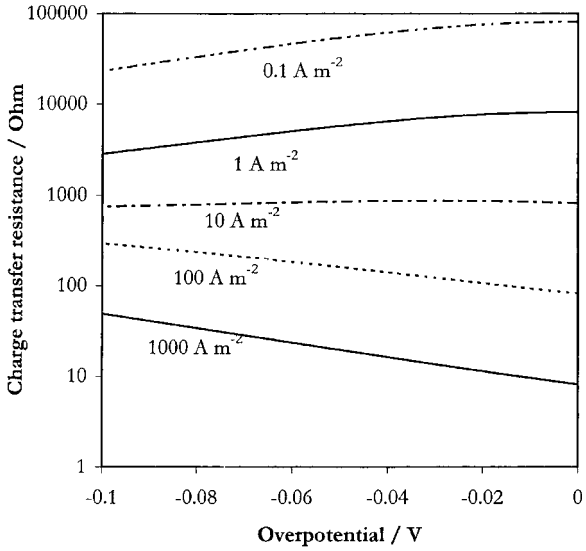

Fig. 6. Calculated variations of the charge transfer resistance with the overpotential, depending on the exchange current density. Rotation rate 300 rpm.

4. Conclusions

The general expression for the electrode impedance was established and could be successfully validated by experiments with a test system. For the case of very fast electrode reactions, the high-frequency loop gives indications of both charge and mass transfer rates. The charge transfer resistance defined as the diameter of this loop, is an increasing function of the absolute overpotential $|\eta|$ for significant diffusion control and fast charge transfer through the electrode. In addition, the overall impedance also increases with $|\eta|$.

The model developed for the case of a RDE could be refined considering more accurate description of mass transfer phenomena, in particular by taking into account convection of the fluid near the electrode surface.

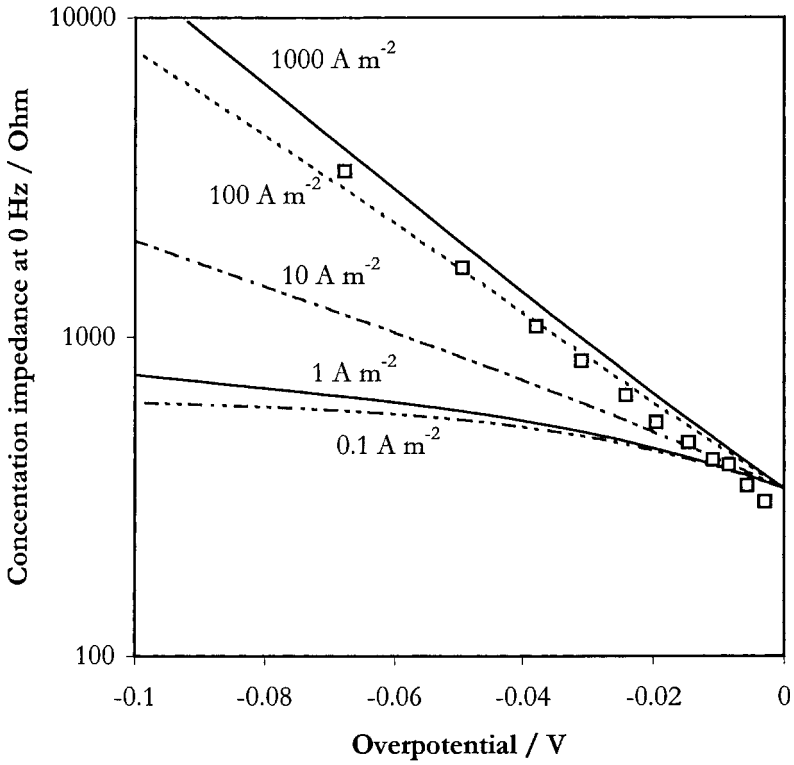

Fig. 7. Calculated variations of the steady-state concentration impedance with the overpotential depending on the exchange current density. Rotation rate 300 rpm. Symbols are for experimental data.

Acknowledgements

The investigation was subsidised by Region Lorraine and CNRS. Thanks are due to Dr Jonathan Deseure for fruitful discussions. The authors are also indebted to the referees for thorough criticism of the manuscript.

References

1. M. Sluyters-Rehbach and J.H. Sluyters, *J. Electroanal. Chem.* **4** (1970) 1.
2. C. Gabrielli, 'Identification of Electrochemical Processes by Frequency Response Analysis' (Solartron Instruments, Farnborough, 1980).
3. J.P. Diard, B. Le Gorrec and C. Montella, 'Cinétique Electrochimique', Hermann (Editeurs des Sciences et des Arts, Paris, 1996).
4. H.H. Girault, 'Electrochimie Physique et Analytique', (Presses Polytechniques et Universitaires Romandes, Lausanne, 2001).
5. U. Retter, A. Widman, K. Sigler and H. Kahlert, *J. Electroanal. Chem.* **546** (2003) 87.
6. J.-P. Diard, N. Glandut, B. Le Gorrec and C. Montella, *J. Electroanal Chem.* (2004), forthcoming.
7. F. Cœuret and A. Storck, 'Eléments de Génie Electrochimique' (Technique & Documentation-Lavoisier, Paris, 1993).
8. J.M. Hornut, F. Lapicque and A. Storck, *Chem. Eng. J.* **43** (1990) 107.
9. K.J. Vetter, Electrochemical Kinetics, 'Theoretical and Experimental Aspects (Academic Press, New York, 1967).
10. K. Winkler, *J. Electroanal. Chem.* **388** (1995) 151.
11. M.E. Orazem, M. Durbha, C. Deslouis, H. Takenouti and B. Tribollet, *Electrochim. Acta* **44** (1999) 4403.
12. E. Levart and D. Schuhmann, *J. Electroanal. Chem.* **122** (1975) 1082.
13. B. Tribollet and J. Newman, *J. Electrochem. Soc.* **130**(4) (1983) 822.
14. D.A. Scherson and J. Newman, *J. Electrochem. Soc.* **127**(1) (1980) 110.
15. P. Zoltowski, *J. Electroanal. Chem.* **443** (1998) 149.